Engineering Structures 49 (2013) 373–384

Contents lists available at SciVerse ScienceDirect

Engineering Structures

journal homepage: www.elsevier.com/locate/engstruct

A parametric study of curved incrementally launched bridges

Michele Fabio Granata *, Piercarlo Margiotta, Marcello Arici

Università di Palermo, DICAM, Palermo, Italy

ARTICLE INFO

Article history:
Received 8 May 2012
Revised 18 September 2012
Accepted 5 November 2012
Available online 25 December 2012

Keywords:
Bridge
Incremental launching
Curved beam
Transfer matrix
Torsion
Parametric study

ABSTRACT

The structural behaviour of incrementally launched bridges in the construction stages depends on different parameters involving deck, nose, supports and guide devices, because static schemes vary continuously with the advance of the deck above the piers. For this reason temporary stresses in the deck, during launching, are rather different from those occurring in service life. Horizontally curved launched bridges also present the effects of torsion induced by geometric curvature. A parametric study is presented in order to analyse the influence of design parameters on the construction of these bridges. Analyses were carried out by extending to curved beams a procedure based on the Transfer Matrix Method, already known for straight continuous decks. Effects of curvature, nose–deck ratios of length and load, bending and torsional stiffness ratio were taken into account. The results show that maximum torsion values increase with the decrease in the curvature radius R and with the decrease in the ratio between bending and torsional stiffness. Moreover, with variation in the nose length ratio, the value $l_n/l = 0.60$ with respect to the span length, is confirmed as the optimal value, as happens for straight bridges. With variation in the nose weight, a significant increase in bending moment and torsion can only be appreciated in the cantilever stages of launching. Dimensionless diagrams and related expressions are given for numerical evaluation of the maximum values of bending moment and torsion in the construction stages, with variation in the stiffness ratio and the radius of curvature.

1. Introduction

Incremental launching of bridges is nowadays a widespread methodology for the construction of continuous bridge decks. It can be applied both to concrete and steel bridge girders and it has the advantage of eliminating the traditional scaffolding to support formwork. This technology requires low investments in specialised equipments such as a launching nose, conventional jacks, launching jacks, temporary slide and guide devices. Deck segments are built in a concentrated working area, placed behind one of the abutments of the bridge, centralizing all concrete or steel construction activities. For concrete bridges, each segment is cast in contact with the previously completed part of the structure, and assembled to it through prestressing. By contrast, steel decks are directly assembled by joining segments with bolted or welded connections. The whole assembled girder is then advanced forward a distance equal to the last segment already built, releasing the working area for the construction of the new segment. The construction sequence is repetitive and may be organised to reach very efficient and high-quality workmanship [1].

From the designer's point of view, an incrementally launched bridge presents different behaviour between the first phase of the project (construction stages) and the second phase (service life). It implies that temporary stresses during launching are different from those occurring at the end of construction and after, when moving loads are applied [2]. In the first phase, for every span launched, a first portion of the deck advances as a cantilever and a steel nose is generally applied to the front of the advancing deck (Fig. 1). In this stage significant negative bending moments appear in the cantilever deck portion, with upper fibres of the deck cross-section in tension. By contrast, when the nose reaches the next pier, positive moments appear in the same segments, advancing as far as the centre of the last span. The nose length is strictly related to the span length and to the girder properties. Due to the different structural behaviour between each construction phase, it is necessary to consider a large number of structural schemes for every position of the deck above the piers during launching, till the final position is achieved. For concrete bridges, the most common deck is composed of a straight single box concrete girder sliding onto the bearings positioned over the piers and pushed from behind. Single box sections are usually preferred in this construction technique because the entire section has a better mechanical performance due to the geometric efficiency coefficient and to its effectiveness in resisting torsion and warping [3]. So, due to the rigidity of the concrete box sections, which are stiffened in the

* Corresponding author. Tel.: +39 3495951848.
E-mail addresses: michelefabio.granata@unipa.it (M.F. Granata), ing.margiotta@gmail.com (P. Margiotta), marcello.arici@unipa.it (M. Arici).

0141-0296/$ - see front matter © 2012 Elsevier Ltd. All rights reserved.
http://dx.doi.org/10.1016/j.engstruct.2012.11.007

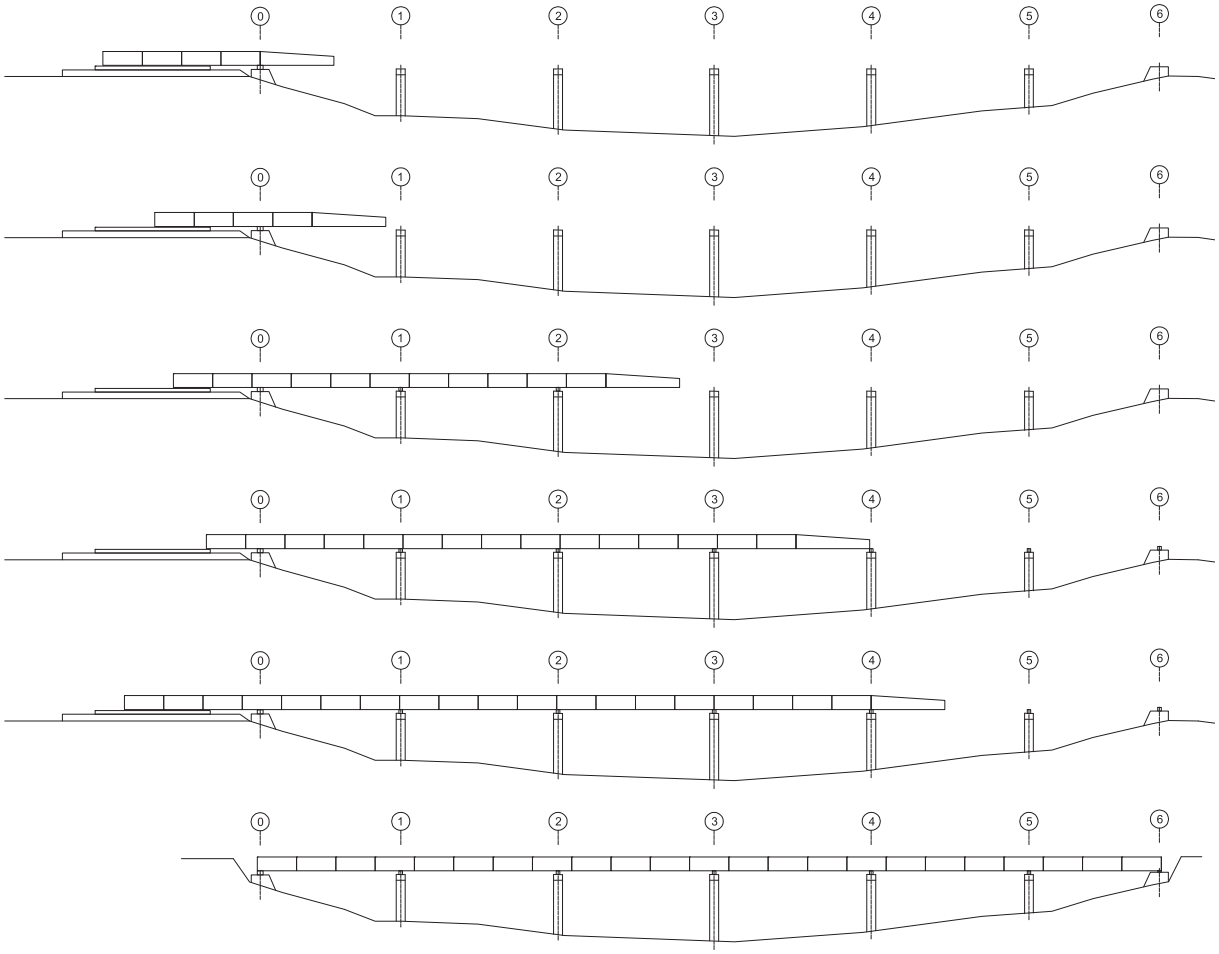

Fig. 1. Stages of incremental launching.

internal corners in most cases, it is possible to assume that beam members are prismatic and that the cross-section does not change shape, neglecting distortion. Nowadays incremental launching is often also used in the construction of I-shaped or box steel girders, even though they require a more diffused system of transverse stiffeners in order to assure the behaviour of a rigid section without distortion [4].

In the case of straight bridges, torsional and bending analyses are uncoupled and torsion is only considered in the second design phase for eccentric moving loads applied in service life. Rosignoli also considers torsion and cross-section distortion when misplacements of launching bearings occur in construction stages [5]. Apart from the case of misplacements, the final scheme of the bridge (in service life) is a continuous beam with the assumption of stiff transverse elements placed along the deck. By contrast, in the construction phase the temporary static scheme is a shorter continuous beam with a cantilever at the end, in which bending moment is the main internal force and governs the structural behaviour. The analysis requires a considerable amount of calculations related to a wide number of support configurations. So it is necessary to analyse the structure for each launching step, which is a tedious and time-consuming process. Rosignoli used the Transfer Matrix Method (TMM) for the analysis of continuous straight bridges during construction, introducing a Reduced Transfer Matrix (RTM) algorithm in the procedure. The method, based on the integration of the elastic beam differential equations, uses a fast and repetitive procedure that limits the risk of mistakes and can easily be implemented in computer software [6].

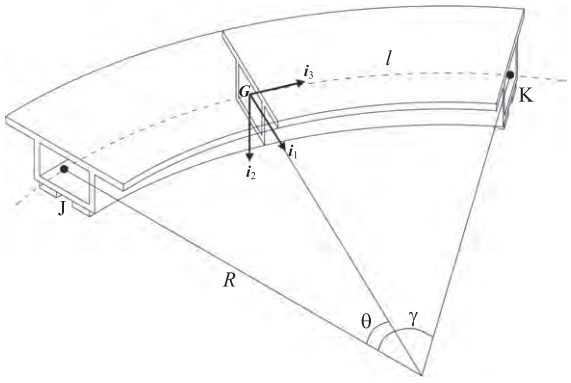

Fig. 2. Curved bridge segment between two piers (segment JK).

When these bridges are curved in plane or both in plane and elevation [7], the deck curvature is generally kept constant. This geometric characteristic implies construction complications because launching bearings, guide devices and pushing methods strictly depend on geometric constraints and in this case radial forces appear at the top of every pier. Moreover, the deck's static behaviour changes, involving torsion both in construction stages and service life. Indeed, while during launching a straight bridge deck only has flexural behaviour, a curved one has mainly flexural behaviour associated with torsion. The general theory of curved box girder bridges can be found in [8]. Engineering practice, for curved bridges with high values of curvature radii, was limited to the evaluation of temporary stresses during construction, curvature being neglected and the equivalent straight bridge being con-

sidered. Nowadays, with the use of Finite Element Method (FEM) it is generally accepted that the bridge curved deck is modelled by a number of straight elements, approximating the real curved geometry. These simplifications can introduce errors in the evaluation of internal forces because they do not adequately consider the role played by torsion. This can have important effects: during launching tangential stresses due to torsion add to those due to shear, while in service life the geometric curvature increases the effects of moving loads.

In the second design phase, regarding service loads (additional permanent and moving loads), final prestressing has to be considered for concrete bridges as well as possible changes of support configuration over piers. Moreover, due to the different cast ages of segments assembled during launching, rheological non-homogeneity occurs in concrete and composite bridges, affecting the state of stress at time t_1 (end of construction) and at time t_∞ (when delayed deformations will have totally developed).

This paper only regards the first design phase with the effects of dead load in the launching sequence. A parametric study of curved incrementally launched bridges is presented (in the paper), based on the Reduced Transfer Matrix (RTM) procedure, firstly applied by Rosignoli to straight continuous beams and then extended to curved concrete box girders by Arici and Granata [9]. Similar studies have been presented by some authors for straight bridges, starting from the paper by Marchetti, who presented an extensive study [1] in which specific design problems related to incrementally launched bridges are considered. Evaluations of bending moments during launching, nose and deck characteristics, applied loads and prestressing requirements are given by this author. Rosignoli also presented studies on nose–deck interaction in launched concrete straight bridges [10] while Sasmal et al. [11] presented a parametric study in which different deck and nose characteristics and different nose/deck load ratios were taken into account for straight launched bridges.

Recently, Fontan et al. [12] presented a study on optimisation of the launching nose in prestressed concrete bridges, in which bending moments over the piers and stress evaluation for the deck cross-section are evaluated in the different positions of the deck during the launching steps.

Mapelli et al. [13] pointed out the effects of delayed deformations and rheological non-homogeneity in concrete bridges built using the incremental launching technique. These authors implemented a mathematical formulation for the evaluation of stresses and deformations, introducing concrete creep into the constitutive laws. They found that the multiple change in the static scheme during launching can affect the final values of bending moments in service life.

In the present study the RTM methodology, extended to horizontally curved bridges, was used to perform parametric analyses. Torsional effects due to the geometric curvature are taken into account, considering only Saint Venant torsion (primary torsion), warping and cross-section distortion being neglected. For box sections, it has been shown [3,4] that effects of non-uniform torsion, in terms of longitudinal stresses, are only present in limited regions where the value of prevented warping is high, as occurs near supports or for thick diaphragms. By contrast, along the beam warping can be disregarded. In a successive study warping and distortion phenomena will be analysed for curved girders, as well as rheological non-homogeneity in concrete and steel–concrete composite bridges (through the AAEM method [14]), by implementing them in the Transfer Matrix Method. The target of the present study is to investigate how the main design parameters related to the girder and to the nose, affect the values and distribution of bending moments and torsion in construction stages. This is important in the design phase for dimensioning the prestressing values and the related tendon layout. Moreover, the evaluation of tangential stresses strictly depends on the torsion values of cross-sections, with the main aim of steel reinforcement being dimensioning. The parameters considered in this study are the following: the radius of curvature, the ratio between flexural and torsional stiffness of the deck, the nose length and the load ratio between the nose and the deck. In this way a wide range of possible girder cross-sections is investigated. The results are given in the form of graphs in order to simplify interpretation of data and to apply the parametric analysis to actual cases of engineering practice, especially for the early design phases of curved launched bridge conceptual design, when choices about bridge deck, nose and launching technology have to be made by designers.

2. Reduced transfer matrix method for curved continuous beams

The theoretical approach to the elastic analysis of complex 3-D prismatic curved structures, using the Transfer Matrix Method, was formulated in [15,16]. The solving system was derived by exact integration of the canonical Hamiltonian system of 12 differential equations, governing the static behaviour in small displacement field. The authors applied this formulation to the analysis of incrementally launched curved box girders through the extended RTM procedure. In the following sections, RTM is stated by writing the fundamental equations in a more compact way than in [9], in order to simplify comprehension of the approach followed.

For a horizontally curved beam whose axis lies on a horizontal plane (See Fig. 2), in the generic section of curvilinear coordinate s, with the local coordinate system given by the Frenet unit vectors $\boldsymbol{i}_1, \boldsymbol{i}_2, \boldsymbol{i}_3$ placed in the cross-section centroid, the mixed state array containing displacement components and internal forces can be defined by

$$\mathbf{z}(s) = \begin{pmatrix} \mathbf{u}(s) \\ \mathbf{Q}(s) \end{pmatrix} = \begin{pmatrix} u_2 \\ \varphi_1 \\ \varphi_3 \\ V_2 \\ M_1 \\ M_3 \end{pmatrix} \tag{1}$$

where u_2 is the vertical displacement, φ_1 the bending rotation, φ_3 the torsional rotation, V_2 the shear force, M_1 the bending moment and M_3 the torsion.

The relation between the state array in $s = 0$ and the one in the generic section of abscissa s, is given by the transfer matrix $\mathbf{C}(s)$:

$$\mathbf{z}(s) = \mathbf{C}(s)\mathbf{z}(0) + \mathbf{N}(s) \tag{2}$$

where $\mathbf{C}(s)$ depends on the geometrical and mechanical characteristics of the beam and $\mathbf{N}(s)$ expresses the effects of external actions along the beam axis. For a horizontal plane curved beam the expression of the transfer matrix can be written:

$$\mathbf{C}(s) = \mathbf{exp}\,(\mathbf{J}\mathbf{A}\,s) = \left[\begin{array}{c|c} \mathbf{Y}(s) & \mathbf{D}(s) \\ \hline \mathbf{0} & \mathbf{Y}^{\mathrm{T}}(-s) \end{array}\right] \tag{3}$$

where $\mathbf{Y}$ and $\mathbf{D}$ are 3×3 sub-matrices of $\mathbf{C}$, $\mathbf{J}$ is the skew symmetric symplectic operator

$$\mathbf{J} = \begin{bmatrix} 0 & \mathbf{I} \\ -\mathbf{I} & 0 \end{bmatrix} \tag{4}$$

while $\mathbf{I}$ is the 3×3 identity matrix and

$$\mathbf{A} = \left[\begin{array}{c|c} \mathbf{0} & -\mathbf{B}^{\mathrm{T}} \\ \hline -\mathbf{B} & \mathbf{E}^{-1} \end{array}\right] = \left[\begin{array}{ccc|ccc} 0 & 0 & 0 & 0 & 0 & 1/R \\ 0 & 0 & 0 & -1 & 0 & 0 \\ 0 & 0 & 0 & 0 & -1/R & 0 \\ \hline 0 & -1 & 0 & \chi_2/GA & 0 & 0 \\ 0 & 0 & -1/R & 0 & 1/EJ_1 & 0 \\ 0 & 1/R & 0 & 0 & 0 & 1/GJ \end{array}\right] \tag{5}$$

Matrix **C** can be obtained numerically, as an exponential matrix, using common mathematical software. In Eq. (5) **B** is the gradient matrix of displacements (referred to the compatibility equations), $\mathbf{E}^{-1}$ is the diagonal flexibility matrix, the inverse of the stiffness matrix and valid for a beam having constant cross-section with an axis of symmetry along $\boldsymbol{i}_2$, R is the constant curvature radius, A is the cross-section area, E is the Young elastic modulus, G is the shear modulus, χ_2 is the shear factor, J_1 is the moment of inertia and J is the torsional constant.

The effects of external actions (distributed loads and imposed strains on the beam) can be taken into account by the array $\boldsymbol{N}(s)$ with the following expression:

$$\boldsymbol{N}(s) = \int_0^s \boldsymbol{C}(s-\eta)\boldsymbol{J}\boldsymbol{d}_e(\eta)d\eta \tag{6}$$

in which

$$\boldsymbol{d}_e(s) = \left[\boldsymbol{f}_e^{\mathrm{T}}(s), \boldsymbol{q}_e^{\mathrm{T}}(s)\right]^{\mathrm{T}} \tag{7}$$

$\boldsymbol{f_e}(s) = (p_2(s), m_1(s), m_3(s))^{\mathrm{T}}$ being the distributed external load array and $\boldsymbol{q_e}(s) = (q_2(s), q_1(s), q_3(s))^{\mathrm{T}}$ the imposed strain array (e.g. imposed curvature induced by a thermal gradient).

Once the transfer matrix $\mathbf{C}(s)$ has been defined, it is possible to expand it by adding one more column and one more row, in order to include $\mathbf{N}(s)$, so in a more compact form the general expression (2) becomes:

$$\mathbf{S}(s) = \begin{pmatrix}\mathbf{z}(s)\\ 1\end{pmatrix} = \left[\begin{array}{c|c} \mathbf{C}(s) & \mathbf{N}(s) \\ \hline \mathbf{0}^{\mathrm{T}} & 1 \end{array}\right]\begin{pmatrix}\mathbf{z}(0)\\ 1\end{pmatrix} = \left[\begin{array}{c|c|c} \mathbf{Y}(s) & \mathbf{D}(s) & \mathbf{N}_{\mathbf{u}}(s) \\ \hline \mathbf{0} & \mathbf{Y}^{\mathrm{T}}(-s) & \mathbf{N}_{\mathbf{Q}}(s) \\ \hline \mathbf{0}^{\mathrm{T}} & \mathbf{0}^{\mathrm{T}} & 1 \end{array}\right]\begin{pmatrix}\mathbf{u}(0)\\ \mathbf{Q}(0)\\ 1\end{pmatrix} = \mathbf{F}(s)\mathbf{S}(0) \tag{8}$$

where $\mathbf{S}(s)$ is the expanded state array and $\mathbf{F}(s)$ is the expanded transfer matrix for the generic section s. The relations written above are valid for each section s along the beam axis. Therefore, the relation between the state arrays of two subsequent sections J and K can be expressed by the 7×7 matrix $\mathbf{F}_{\mathrm{J}}^{\mathrm{K}}$:

$$\mathbf{S}_{\mathrm{K}} = \mathbf{F}_{\mathrm{J}}^{\mathrm{K}}\mathbf{S}_{\mathrm{J}} \tag{9}$$

More details about transfer matrices of curved elements subjected to different actions (distributed and concentrated loads, imposed strains and displacements, temperature loads) are given in [9,16].

Let us consider a circular curved continuous beam on rigid radial supports with constant curvature radius R. In this case $s = R\theta$ is the curvilinear coordinate of the generic section and $L = R\omega$ the total beam length from 0 to 1 (Fig. 3), with several spans each of length $l_{\mathrm{JK}} = R\gamma_{\mathrm{JK}}$ between two subsequent supports J and K.

In each support section a point matrix $\mathbf{P}_{\mathrm{K}}$ can be defined to take into account concentrated discontinuities due to support reactions. The 7th order matrix $\mathbf{P}_{\mathrm{K}}$ is composed of a 6th order identity matrix and of a 7th order column containing the terms of concentrated discontinuities:

$$\mathbf{P}_{\mathrm{K}} = \begin{bmatrix} 1 & 0 & 0 & 0 & 0 & 0 & \Delta u_2 \\ 0 & 1 & 0 & 0 & 0 & 0 & \Delta\varphi_1 \\ 0 & 0 & 1 & 0 & 0 & 0 & \Delta\varphi_3 \\ 0 & 0 & 0 & 1 & 0 & 0 & \Delta V_2 \\ 0 & 0 & 0 & 0 & 1 & 0 & \Delta M_1 \\ 0 & 0 & 0 & 0 & 0 & 1 & \Delta M_3 \\ 0 & 0 & 0 & 0 & 0 & 0 & 1 \end{bmatrix} \tag{10}$$

By considering discontinuities over supports, the state array at the end section of the curved beam can be expressed by the recursive formula:

$$\mathbf{S}_1 = \mathbf{F}_0^1\mathbf{S}_0 = \mathbf{F}_{\mathrm{N}}^1\mathbf{P}_{\mathrm{N}}\mathbf{F}_{\mathrm{N}-1}^{\mathrm{N}}\mathbf{P}_{\mathrm{N}-1}\ldots\mathbf{F}_{\mathrm{A}}^{\mathrm{B}}\mathbf{P}_{\mathrm{A}}\mathbf{F}_0^{\mathrm{A}}\mathbf{S}_0 \tag{11}$$

Each matrix $\mathbf{P}_{\mathrm{K}}\mathbf{F}_{\mathrm{J}}^{\mathrm{K}}$, obtained by the product of the support point matrix $\mathbf{P}_{\mathrm{K}}$ and the span-by-span matrix $\mathbf{F}_{\mathrm{J}}^{\mathrm{K}}$, contains only two redundant unknowns (support reaction discontinuities ΔV_2 and ΔM_3), because the other concentrated discontinuities have null values. Thus relation (11) contains all the redundant unknowns of the continuous beam. Without considering these unknowns, the solution is given by a system of six equations with 12 unknowns. Six equations can be found by imposing the boundary conditions in the state arrays of the two end sections. Redundant unknowns require the definition of an equal number of auxiliary conditions that can be found by calculating the state arrays at the support sections, imposing in them null values of vertical displacements and torsional rotations (compatibility equations). The number of redundant reactions, and consequently of auxiliary conditions, increases with the advancing of the deck above new piers involved during launching. In order to avoid this problem another pathway can be followed by improving the TMM and only operating on the two continuous elements of state arrays and transfer matrices (bending rotations and bending moments), obtaining a reduced system, using the procedure which will now be described.

A partition of matrix $\mathbf{F}_{\mathrm{J}}^{\mathrm{K}}$ can be performed by considering arrays $\mathbf{K}_{\mathrm{J}} = (u_2\phi_3)_{\mathrm{J}}^{\mathrm{T}}$ and $\mathbf{K}_{\mathrm{K}} = (u_2\phi_3)_{\mathrm{K}}^{\mathrm{T}}$ of known variables at support sections, arrays $\mathbf{U}_{\mathrm{J}} = (V_2M_3)_{\mathrm{J}}^{\mathrm{T}}$ and $\mathbf{U}_{\mathrm{K}} = (V_2M_3)_{\mathrm{K}}^{\mathrm{T}}$ of unknown variables and arrays $\mathbf{z}_{\mathbf{RJ}} = (\phi_1M_1)_{\mathrm{J}}^{\mathrm{T}}$ and $\mathbf{z}_{\mathbf{RK}} = (\phi_1M_1)_{\mathrm{K}}^{\mathrm{T}}$ of continuous variables upon each support. For continuous variables, the values at the left and right sides of an internal support must be the same for equilibrium and compatibility conditions. The transfer matrix of a span J–K can be rearranged in the following way:

$$\begin{pmatrix}\mathbf{K}_{\mathrm{K}}\\ \mathbf{U}_{\mathrm{K}}\\ \mathbf{z}_{\mathbf{RK}}\\ 1\end{pmatrix} = \begin{bmatrix}\mathbf{F}_{11} & \mathbf{F}_{12} & \mathbf{F}_{13} & \mathbf{F}_{14}\\ \mathbf{F}_{21} & \mathbf{F}_{22} & \mathbf{F}_{23} & \mathbf{F}_{24}\\ \mathbf{F}_{31} & \mathbf{F}_{32} & \mathbf{F}_{33} & \mathbf{F}_{34}\\ 0^{\mathrm{T}} & 0^{\mathrm{T}} & 0^{\mathrm{T}} & 1\end{bmatrix}\begin{pmatrix}\mathbf{K}_{\mathrm{J}}\\ \mathbf{U}_{\mathrm{J}}\\ \mathbf{z}_{\mathbf{RJ}}\\ 1\end{pmatrix} \tag{12}$$

From the first row of Eq. (12), by solving with respect to the unknown elements $\mathbf{U}_{\mathrm{J}}$,

$$\mathbf{U}_{\mathrm{J}} = \mathbf{F}_{12}^{-1}(\mathbf{K}_{\mathrm{K}} - \mathbf{F}_{11}\mathbf{K}_{\mathrm{J}} - \mathbf{F}_{13}\mathbf{z}_{\mathbf{RJ}} - \mathbf{F}_{14}) \tag{13}$$

while, from the third row of Eq. (12), one obtains

$$\mathbf{z}_{\mathbf{RK}} = \mathbf{G}_{\mathrm{J}}^{\mathrm{K}}\mathbf{z}_{\mathbf{RJ}} + \mathbf{G}_{\mathbf{NJ}}^{\mathrm{K}} \tag{14}$$

in which

$$\begin{aligned}\mathbf{G}_{\mathrm{J}}^{\mathrm{K}} &= \mathbf{F}_{33} - \mathbf{F}_{32}\mathbf{F}_{12}^{-1}\mathbf{F}_{13}\\ \mathbf{G}_{\mathbf{NJ}}^{\mathrm{K}} &= \mathbf{F}_{31}\mathbf{K}_{\mathrm{J}} + \mathbf{F}_{32}\mathbf{F}_{12}^{-1}(\mathbf{K}_{\mathrm{K}} - \mathbf{F}_{11}\mathbf{K}_{\mathrm{J}} - \mathbf{F}_{14}) + \mathbf{F}_{34}\end{aligned} \tag{15}$$

By inserting $\mathbf{G}_{\mathbf{NJ}}^{\mathrm{K}}$ and $\mathbf{G}_{\mathrm{J}}^{\mathrm{K}}$ into a reduced transfer matrix $\mathbf{F}_{\mathbf{RJ}}^{\mathrm{K}}$

$$\mathbf{F}_{\mathbf{RJ}}^{\mathrm{K}} = \begin{bmatrix}\mathbf{G}_{\mathrm{J}}^{\mathrm{K}} & \mathbf{G}_{\mathbf{NJ}}^{\mathrm{K}}\\ 0^{\mathrm{T}} & 1\end{bmatrix} \tag{16}$$

and by considering the reduced state array $\mathbf{S}_{\mathbf{R}} = (\varphi_1\ M_1\ 1)^{\mathrm{T}}$, a more compact expression of Eq. (14) can be found, obtaining a reduced system

$$\mathbf{S}_{\mathbf{RK}} = \mathbf{F}_{\mathbf{RJ}}^{\mathrm{K}}\mathbf{S}_{\mathbf{RJ}} = \begin{bmatrix}\mathrm{F}_{\mathrm{R}11} & \mathrm{F}_{\mathrm{R}12} & \mathrm{F}_{\mathrm{R}13}\\ \mathrm{F}_{\mathrm{R}21} & \mathrm{F}_{\mathrm{R}22} & \mathrm{F}_{\mathrm{R}23}\\ 0 & 0 & 1\end{bmatrix}_{\mathrm{J}}^{\mathrm{K}}\begin{pmatrix}\varphi_1\\ M_1\\ 1\end{pmatrix}_{\mathrm{J}} \tag{17}$$

where $\mathbf{F}_{\mathbf{RJ}}^{\mathrm{K}}$ is the 3×3 *reduced transfer matrix* of the JK segment between two subsequent supports. Eq. (15) show that elements of reduced transfer matrix $\mathbf{F}_{\mathbf{RJ}}^{\mathrm{K}}$ are obtained directly as a combination of those of transfer matrix $\mathbf{F}_{\mathrm{J}}^{\mathrm{K}}$. In this way, if the segment of the continuous beam between A and N (Fig. 3) is considered, the reduced solving system is:

$$\mathbf{S}_{\mathbf{RN}} = \mathbf{F}_{\mathbf{RA}}^{\mathrm{N}}\mathbf{S}_{\mathbf{RA}} = \mathbf{F}_{\mathbf{RN}-1}^{\mathrm{N}}\mathbf{F}_{\mathbf{RN}-2}^{\mathrm{N}-1}\ldots\mathbf{F}_{\mathbf{RA}}^{\mathrm{B}}\mathbf{S}_{\mathbf{RA}} \tag{18}$$

The reduced system of Eq. (11) for the whole continuous curved beam can be solved by imposing the boundary conditions at joints

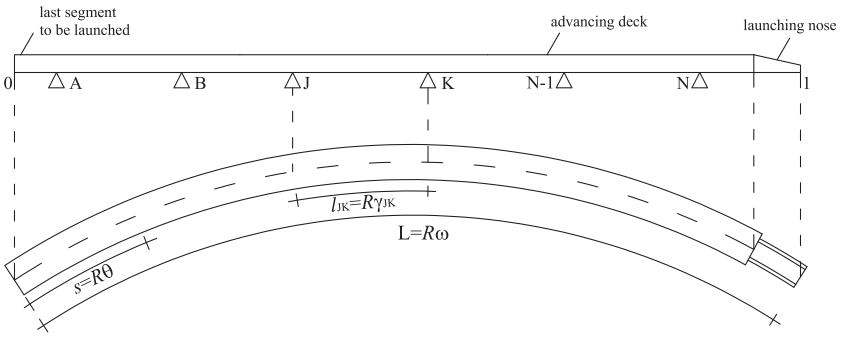

Fig. 3. Continuous curved beam during launching.

A and N (known values of bending moments). After the reduced system is solved, all bending moments and rotations for every support can be found by means of relation (18).

By substituting the values of $\mathbf{S_{RJ}}$ and $\mathbf{S_{RK}}$ in Eq. (12) the continuous beam can be finally solved by defining the complete system of Eq. (11) and the state arrays $\mathbf{S_J}$ and $\mathbf{S_K}$ can be found for each girder segment.

3. Assumptions for the parametric study

A parametric study is presented, based on the results obtained by the analyses of incrementally launched curved girders. A computer program was developed on the basis of the RTM procedure previously explained, in order to find the internal forces of the continuous deck in all construction stages. This procedure has been already validated through a numerical comparison with the Finite Element Method [9], showing a better precision for torsion values with respect to the curved geometry approximated by straight finite elements.

In this parametric study, the effects of curvature, deck and nose characteristics on bending moment and torsion are considered, in order to provide engineers with an efficient tool for the conceptual design of these bridges. The basic layout on which analyses are performed is given by a curved bridge 220 m long (Fig. 4) with a variable curvature radius (when radius $R \to \infty$, a curved bridge degenerates to a straight one with the same span lengths). In its final configuration the bridge has five spans: the central three of equal length (l = 48 m), and two side spans having a length fixed as approximately 80% of the central one (l = 38 m). This choice is related to the advantage of obtaining comparable bending moment values in every span: the optimal ratio between side spans and central ones for long continuous bridges with uniformly distributed loads is about 0.7–0.8 [3]. The bridge is only subjected to dead load, which is assumed to be uniformly distributed both on the deck and on the nose. Evaluations of the effects of other loads like temperature and bearing settlements are given in [9], while effects of prestressing in concrete decks are considered by Sasmal and Ramanjaneyulu [17] and Rosignoli [2] for straight bridges and by Calgaro and Virlogeux [3] and Manterola Armisen [4] for curved bridges. Temporary concrete cracking of upper slabs, delayed deformations due to creep and support misplacements are not considered in the curved bridge, for the first phase of design analysed here. Effects of prestressing have to be evaluated after the preliminary design phase, because a first dimensioning of prestressing force is necessary, due to the bending moment diagram of permanent loads applied in the launching stages. For the nose, which usually consists of a variable cross-section, in the computational procedure average constant properties are assumed.

Because of the need to compensate bending moments on the deck, during launching an auxiliary compensation span (20 m long) is put behind the abutment from which the deck is pushed. Hence during launching the total reference length of the deck is L_{tot} = 240 m.

The parameters considered in the study are:

(1) The radius of curvature R, varying between R = 100 m and R = 500 m.
(2) The ratio between bending stiffness and primary torsional stiffness $k = EJ_1/GJ$, varying from k = 1 to k = 100. The values of k considered here are related to four kinds of typical cross-sections, all stiffened by internal rigid diaphragms, keeping the deck width of 10 m constant:
   - a single concrete box section (Fig. 4d) for which k can be considered not very different than 1;
   - a single steel box section with a concrete slab (Fig. 4e) for which k is about 5;
   - a double steel I girder with a concrete slab (Fig. 4f) for which k is about 50;
   - a double concrete T girder with a top slab (Fig. 4g) for which k is about 100.
(3) The ratio between the nose length l_n and the span length (l = 48 m) varies from the value l_n/l = 0.3 to the value l_n/l = 0.8.
(4) The ratio between the nose load q_n and the deck load q, varies from q_n/q = 0.03 to q_n/q = 0.2.

The results were obtained neglecting warping due to torsion and cross-section distortion for all section typologies, though the solution shows less precision in the cases of Fig. 4f and g, because only primary torsion is considered. All supports are fixed both for vertical displacements and torsional rotations. The latter assumption is the most realistic one, because during launching a double support is generally placed on the pier, especially for curved girders, in order correctly to guide deck advancement and to avoid horizontal girder misplacements. A double support at the pier section constitutes a torsional fixed restraint, but the final pier support can be modified, becoming a single bearing placed at the centre of the deck cross-section (Fig. 5). If, after construction, the restraint conditions vary from the double bearing to the single one on each pier, then torsion is only fixed during launching and released for service loads [4,18]. In the latter case torsion has to be considered a continuous variable on supports in the reduced transfer matrix system of Eqs. (12) and (18).

As previously stated about the service life, these possible changes of support configuration have to be taken into account as well as the effects of final prestressing, moving loads and time-dependent phenomena, considering rheological non-homogeneity for the determination of internal forces at the two times of analysis (t_1 and t_∞).

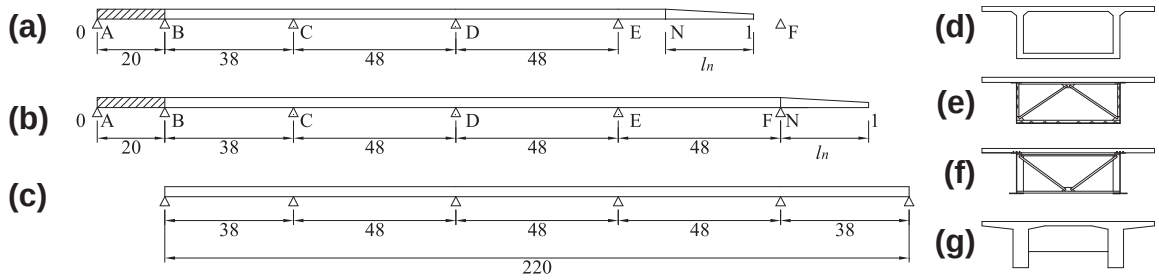

Fig. 4. Bridge launching and typical deck cross-sections. (a) EF span launching before the nose reaches the pier. (b) Launch completed over EF span. (c) Bridge in its final configuration. (d) Concrete box. (e) Steel box with concrete slab. (f) Steel I girders with concrete slab. (g) Concrete T girders with top slab.

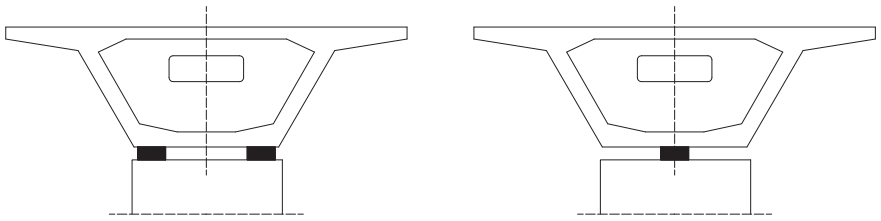

Fig. 5. Support conditions over pier: double bearing, single central bearing.

4. Discussion of parametric study results

The RTM procedure was applied to the launching phases of the reference bridge 4th span (from support E to F). The launching course is analysed in two subsequent stages: the first one is the phase with five supports until the nose reaches pier F, while the second one is the phase with a new support until the joint section between deck and nose reaches pier F (Fig. 4b).

In Fig. 6, the results for the entire launching course are shown in terms of launching subsequent diagrams [6] for bending moment and torsion. These diagrams are obtained by solving the continuous beam during launching for every advancing step over piers (with steps of 2 m) and presenting them with respect to the bridge length at the end of the launching phase, shifting the diagrams in the final position of the deck launched. Fig. 6 shows the superposition of bending moment diagrams and torsion diagrams for the entire launch of the EF span until the joint section between deck and nose reaches the pier.

The envelope bending moment diagram (Fig. 7) is useful for calculating prestressing forces for the launching phase. Prestressing plays a fundamental role in conceptual design of concrete bridges because it is rather different in this stage from that occurring in service. In this connection, for different launching stages, when the deck advances over piers, sections are alternatively subjected to positive and negative moments. So it is common practice to use temporary prestressing tendons in order to reduce stresses by centred prestressing (uniform compression) and to accept limited temporary cracking of concrete in tension. Prestressing tendons configuration can be modified, once the bridge is in its final position, with the final tendons dimensioned for service life [1,2,19].

Torsion shows its maximum and minimum values in the segments behind the nose and these values are very different from those occurring in the rest of the beam. In this case an evaluation of tangential stresses due to shear and torsion in concrete box sections shows an increment with respect to the case of the equivalent straight beam in which there is no torsion. This increment is about 20% in the section with the maximum torsion value while it is about 5–10% in the current sections of the beam.

The evolution of load effects in particular cross-sections can be considered through bending moment and torsion diagrams at support E section (over the pier) during the entire launching course from E to F. This evaluation is useful in order to modify and optimise nose characteristics through fast repetitive calculation of internal forces in different hypotheses of nose length and mechanical properties [10,12].

Fig. 7 shows the envelope diagrams with variation in the curvature radius R, the other parameters being kept constant: $k = 1$ (typical of a box concrete cross-section, Fig. 4d), $l_n/l = 0.6$ and $q_n/q = 0.10$. The diagrams show that, in this case, with variation in the curvature radius, the bending moment can be considered approximately the same. By contrast, the torsion varies significantly, especially in the most advanced part of the deck due to the influence of the cantilever segment of the beam. Naturally, the higher the curvature radius R, the lower the torsion value in every section of the deck, being null for $R \to \infty$. The increment in torsion maximum value for $R = 100$ m with respect to the case of $R = 500$ m is about fivefold. This result was found keeping the stiffness ratio $k = 1$ constant. The fact is that in this case bending moment variation can be neglected but torsion increases can be significant for a small curvature radius.

Fig. 8 shows the diagrams of bending moment and torsion over pier E, during launching of the EF span. The trend is the same as just seen: while in the bending moment diagram no variation is evident, the torsion varies significantly. This happens in the cantilever stage before contact between the nose and pier F and also in the continuous beam stage until the entire span has been launched. When the nose reaches the pier, a big jump in torsion values can be seen for small radii.

Fig. 9 shows the same diagrams as previously seen for a different stiffness ratio ($k = 100$). Higher maximum bending moment values can be noted than those seen in the previous case, against smaller maximum torsion values. The same behaviour is shown by the diagrams in Fig. 10, in which a variation in bending moment values with radius R is observed over the support, after the nose reaches the pier.

Fig. 11 shows the envelope diagrams with variation in the stiffness ratio $k = EJ_1/GJ$, the other parameters $R = 100$ m, $l_n/l = 0.6$, $q_n/q = 0.10$ being kept constant.

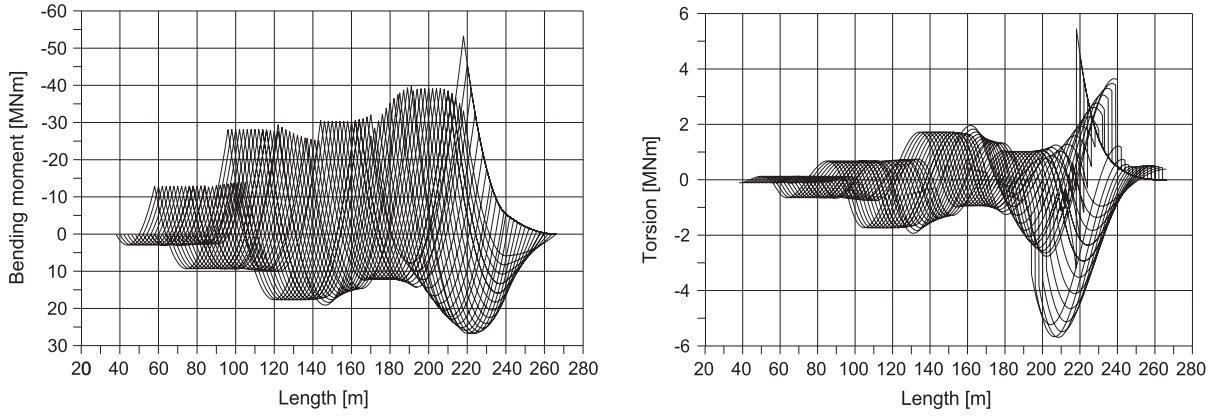

Fig. 6. Envelope bending moment and torsion diagrams for entire launching course over EF span.

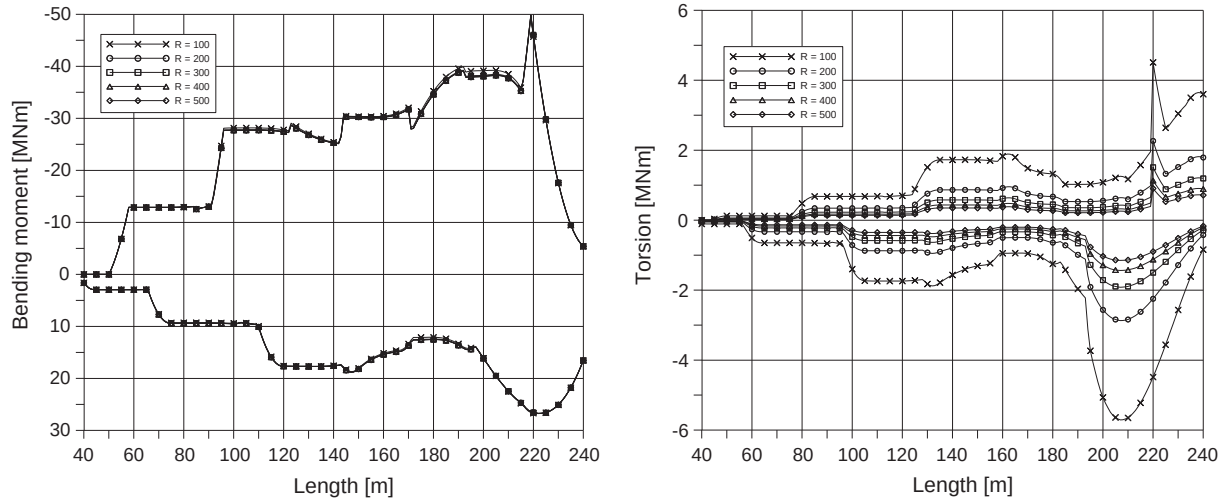

Fig. 7. Bending moment and torsion envelope diagrams, with variation in radius R, when $k = 1$, $l_n/l = 0.6$ and $q_n/q = 0.10$.

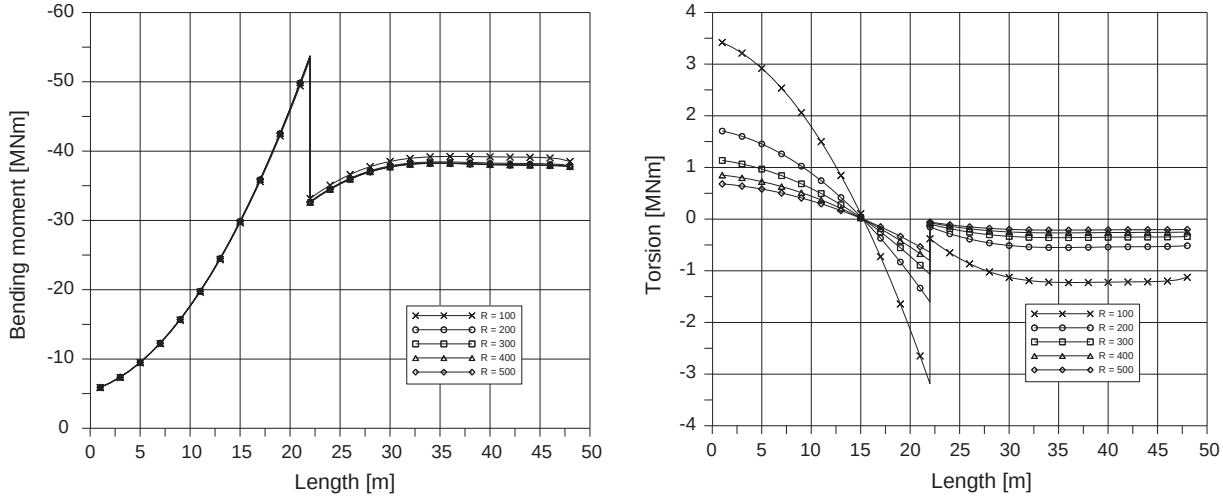

Fig. 8. Bending moment and torsion over the pier, with variation in curvature radius R, when $k = 1$, $l_n/l = 0.6$ and $q_n/q = 0.10$.

In this case the variation in bending moment diagrams is more evident than in the previous ones, the increment in torsion for lower stiffness ratios also being significant. This behaviour shows that, for higher values of k, the torsion diminishes but the bending moment increases. The same behaviour can be appreciated from Fig. 12, which shows diagrams in the support section. While in the cantilever stage, the bending moment does not change after the nose reaches the pier, the bending moment increases and this increment is higher for cross-sections with higher values of k (section types of Fig. 4f and g). By contrast, the torsion varies before

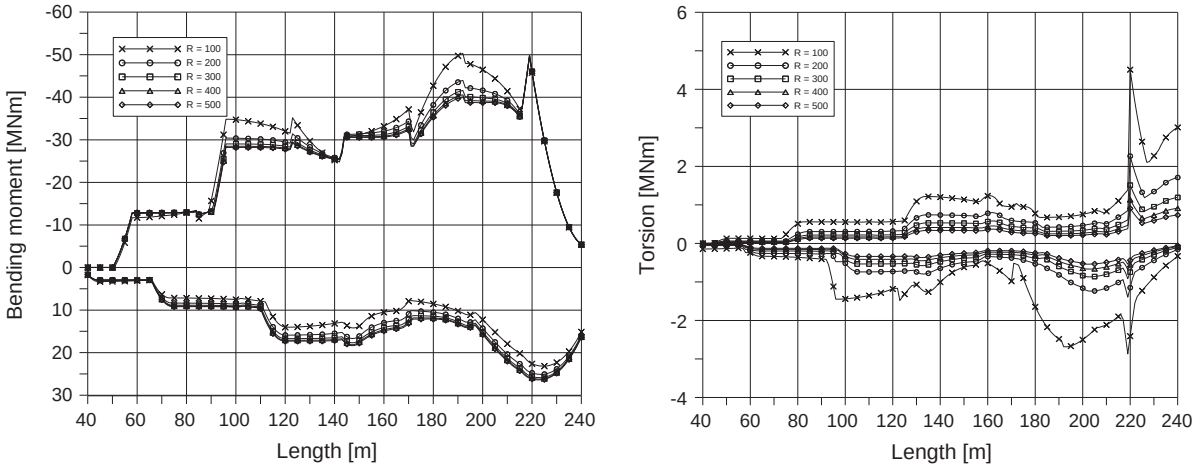

Fig. 9. Bending moment and torsion envelope diagrams, with variation in radius R, when $k = 100$, $l_n/l = 0.6$ and $q_n/q = 0.10$.

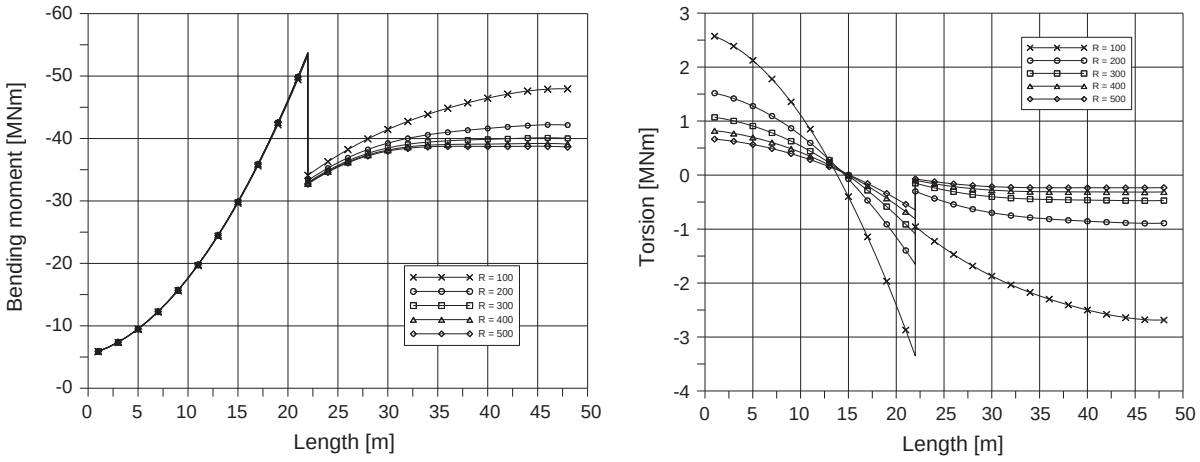

Fig. 10. Bending moment and torsion over the pier, with variation in curvature radius R, when $k = 100$, $l_n/l = 0.6$ and $q_n/q = 0.10$.

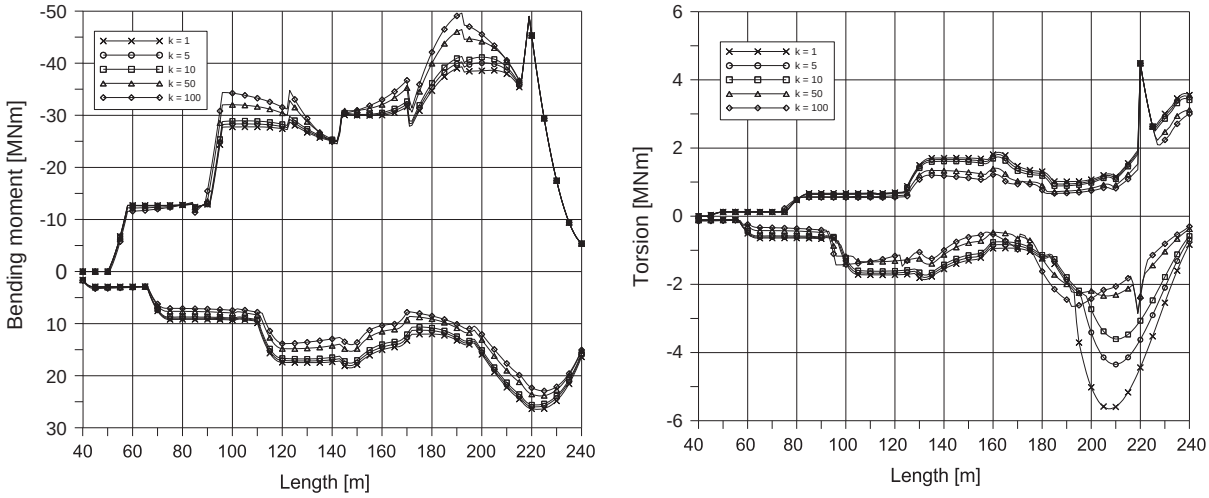

Fig. 11. Bending moment and torsion envelope diagrams, with variation in stiffness ratio k, for $R = 100$ m, $l_n/l = 0.6$ and $q_n/q = 0.10$.

and after contact with the pier, but for high values of k its increment at the end of the launch is more significant.

When R diminishes, torsion becomes more important. When the stiffness ratio changes, bending moment diagrams also change and the torsion depends on curvature and stiffness. The stiffness ratio has a great influence on axial and tangential stresses and governs the structural conception during launching phases: a bending moment diagram allows designers to calculate prestressing forces and tendon configuration, while torsion values are useful for web thickness and stiffener dimensioning.

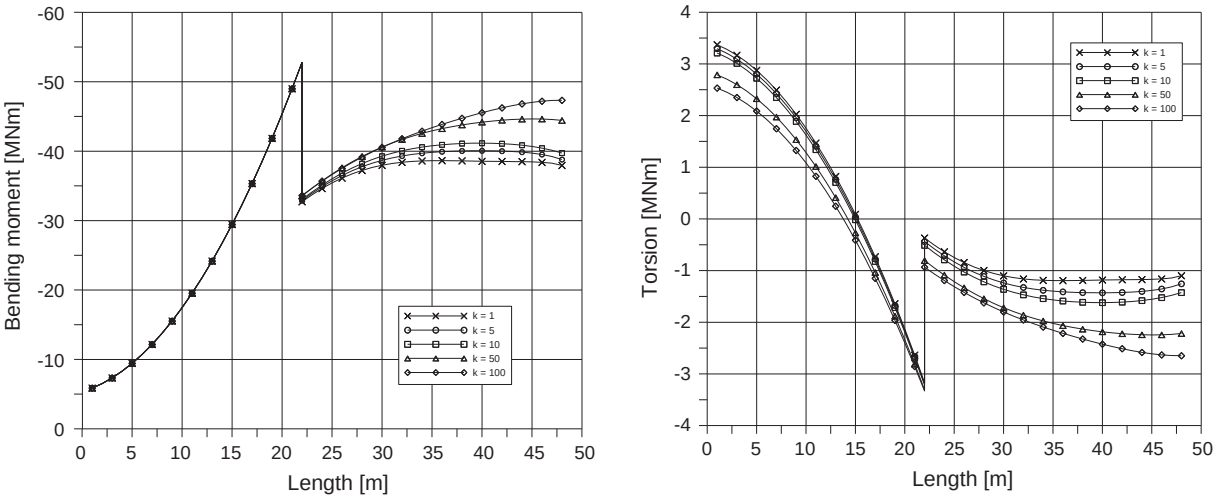

Fig. 12. Bending moment and torsion over the pier, with variation in stiffness ratio k, for $R = 100$ m, $l_n/l = 0.6$ and $q_n/q = 0.10$.

The previous evaluations strictly regard the deck and its characteristics, the nose–deck interaction not being considered. For structural behaviour during launching, a fundamental role is played by the characteristics of the nose with respect to the deck.

Fig. 13 shows the envelope diagrams with variation in the length ratio l_n/l, the other parameters $R = 100$ m, $k = 1$ and $q_n/q = 0.10$ being kept constant. In this case it is evident that a shorter nose significantly increases the cantilever stage during launching. Negative bending moments for the case $l_n/l = 0.30$ can become double with respect to the case $l_n/l = 0.60$. Torsion increases too, but this change is only evident in the cantilever part of the deck during launching.

Fig. 14 shows the diagrams in the support section. For shorter noses the jump and the maximum value increase both for bending moment and torsion. The most adequate value appears to be $l_n/l = 0.60$, because internal forces before and after contact with the pier show similar values. Many authors [1,10,11] indicate this length ratio as the optimal one for straight bridges. The evaluation of torsion effects in horizontally curved beams confirms the same length ratio value. It is worth noting that for longer noses ($l_n/l = 0.80$), internal force values after contact with the pier are higher than before contact. These values are not very different than those found for $l_n/l = 0.60$, though the maximum is related, in the latter case, to the cantilever segment of the deck. This evaluation can differ a lot when concrete decks for railway bridges are considered, because they are much heavier than road bridges with thicker cross-section slabs, in some cases making an increased l_n/l ratio necessary, in order to reduce bending moments in cantilever stages.

Fig. 15 shows the envelope diagrams with variation in the load ratio q_n/q, the other parameters being kept constant: $R = 100$ m, $k = 1$ and $l_n/l = 0.60$. Naturally, with an increase in the load acting on the nose, the cantilever forces increase. This change is not very evident in the envelope diagrams. It is more evident evaluating Fig. 16, which instead shows greater significance for the support internal forces: with an increase in the nose load, the cantilever stage forces and the jump in the diagrams increase significantly. Deck sections passing over the pier during advancing movements are subjected to higher forces for higher nose loads.

This evaluation was made for a fixed value of stiffness ratio and length ratio. It is to be noted that a reduction in nose dead load also influences the bending and torsional stiffness of the nose. This can give an additional effect on internal force distribution. Some authors [1,11], varying the flexural stiffness of the nose together with its load and length ratios, found optimal values of q_n/q for the bending moment in straight bridges.

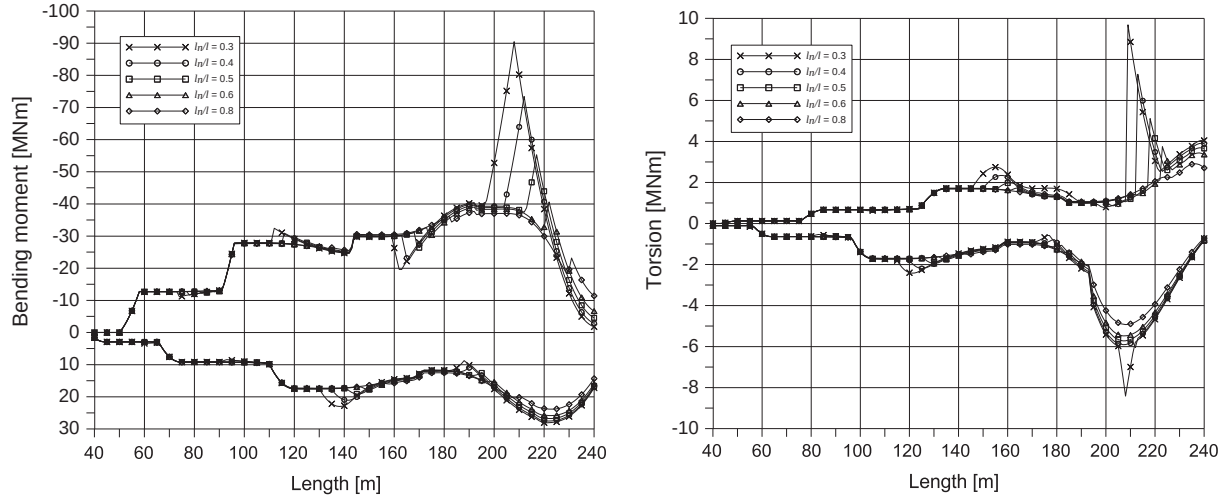

Fig. 13. Bending moment and torsion envelope diagrams, with variation in length ratio l_n/l, for $R = 100$ m, $k = 1$ and $q_n/q = 0.10$.

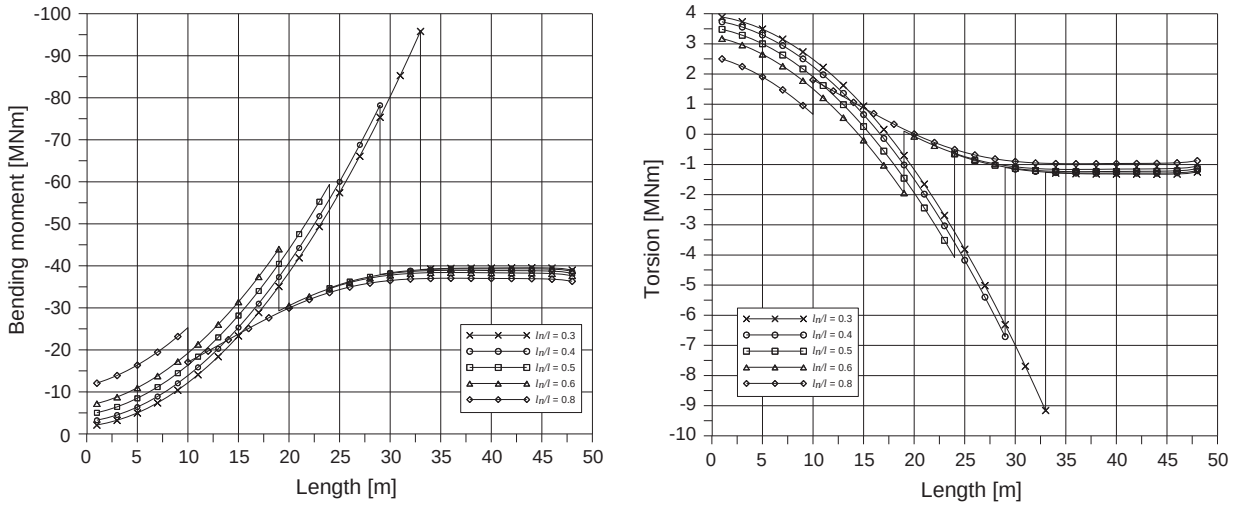

Fig. 14. Bending moment and torsion over the pier, with variation in length ratio l_n/l, for $R = 100$ m, $k = 1$ and $q_n/q = 0.10$.

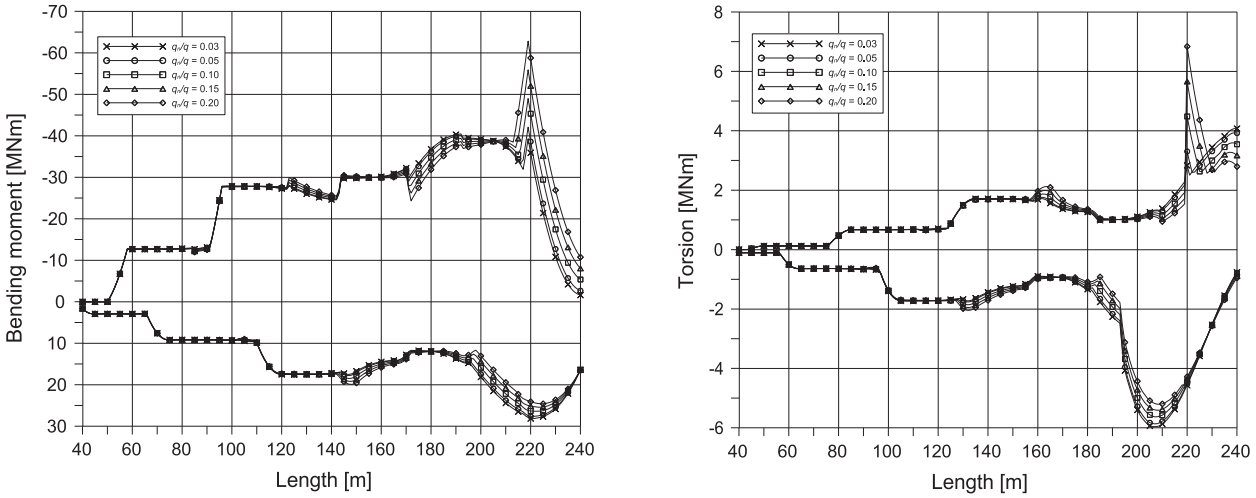

Fig. 15. Bending moment and torsion envelope diagrams, with variation in load ratio q_n/q, for $R = 100$ m, $k = 1$ and $l_n/l = 0.60$.

Fig. 17 shows the dimensionless regression curves of bending moment and torsion maximum values as functions of the stiffness ratio k, for each case of curvature radius R investigated.

Fig. 17a shows that the bending moment remains almost constant with radius R when $k = 1$ (concrete box section), but varies with the radius of curvature when a different stiffness ratio is investigated, confirming what is observed from Fig. 7. Moreover, the maximum value of positive bending moment refers to the case of $k = 1$. The largest variation in maximum bending moment can be observed for the case of $R = 100$ m while the smallest variation is recorded for $R = 500$ m, being null for the case of $R \to \infty$ (straight girder). The minimum value of bending moment is constant for each case examined, being the negative value occurring in the longest cantilever during construction.

The regression curves, for fixed values of $l_n/l = 0.6$ and $q_n/q = 0.10$ can be expressed for bending moments by a second order parabola, as a function of the stiffness ratio k:

$$\frac{Ml}{EJ_1} = ak^2 + bk + c \tag{19}$$

in which M is the maximum value of bending moment, l the length of the longest bridge span, and EJ_1 the bending stiffness ratio of the girder cross-section.

Values of coefficients a, b and c can be found by means of the following expressions:

$$a = 0.0059R^{-2.50};\ b = -0.0390R^{-1.73};\ c = 0.00502 \quad \text{with } R \text{ in [m]} \tag{20}$$

For concrete box sections Eq. (19) becomes $M = (a + b + c)EJ_1/l$.

Fig. 17b shows that torsion values vary significantly with the stiffness ratio k and the curvature R. The diagrams give the maximum negative torsion values, the maximum positive value being almost constant and referring to the longest cantilever stage. The largest variation refers to the case of $R = 100$ m, as happens for bending moments. The highest torsion value is found for the case of concrete box sections with $R = 100$ m.

The torsion regression curves can be expressed as power functions:

$$\frac{M_t l}{EJ_1} = ak^b \tag{21}$$

in which M_t is the maximum torsion value. The values of coefficients a and b can be found using the following expressions:

$$a = 0.113R^{-1};\ b = -0.5R^{-0.17} \quad \text{with } R \text{ in [m]} \tag{22}$$

For concrete box sections Eq. (21) becomes $M_t = 0.113\ EJ_1/(Rl)$.

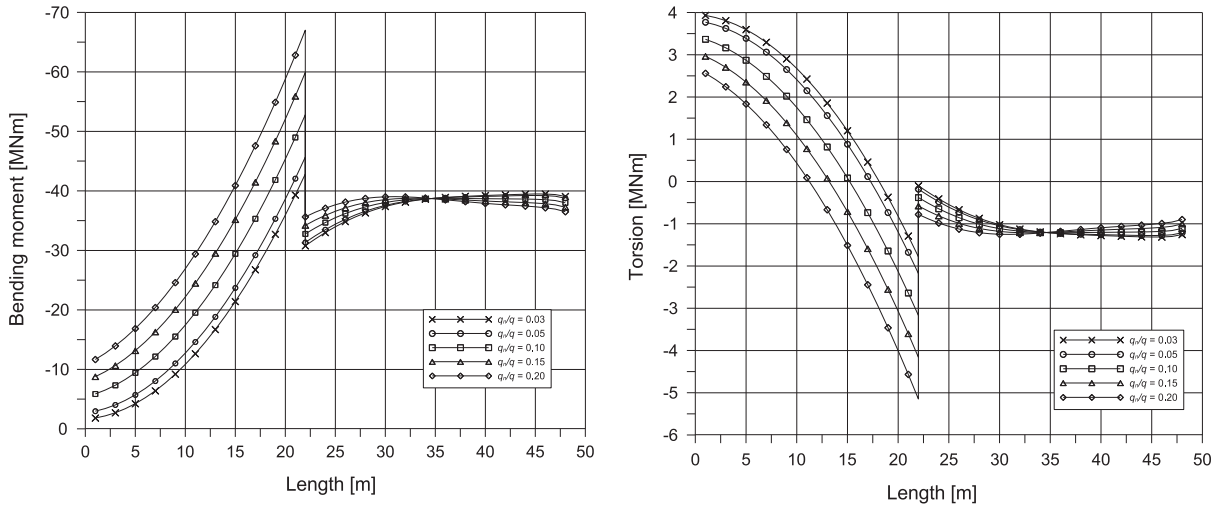

Fig. 16. Bending moment and torsion over the pier, with variation in load ratio q_n/q, for R = 100 m, k = 1 and l_n/l = 0.60.

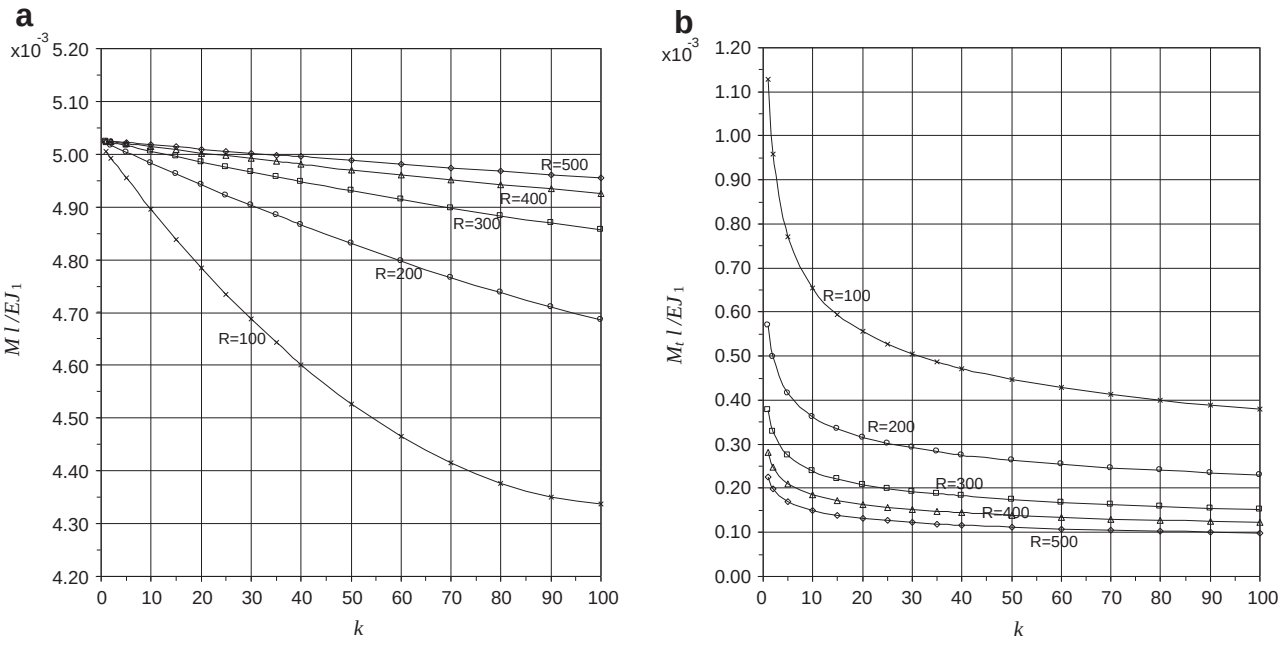

Fig. 17. Variation of maximum values of bending moment and torsion with stiffness ratio k, for fixed values of curvature radius R when l_n/l = 0.6 and q_n/q = 0.10.

The dimensionless curves in Fig. 17 can be useful for design purposes, because they give the maximum values of bending moment and torsion by entering the graph with the values of k and R.

5. Conclusions

A parametric study for the construction sequence of curved incrementally launched bridges was carried out. The procedure followed was based on the reduced transfer matrix method, already known in the literature for straight bridges and extended by the authors to curved continuous beams.

From this parametric study, indications for the conceptual design of curved incrementally bridges can be obtained.

(1) Torsion shows its maximum and minimum values in the span just behind the nose and these values are very different from those occurring in the rest of the beam. An evaluation of tangential stresses due to shear and torsion, in concrete box sections, shows an increment of about 15–20% with respect to the case of the equivalent straight beam in which there is no torsion. This occurs in the span behind the nose, while the increment in tangential stresses is from 5% to 10% in the current sections of the beam. The highest torsion values are found with shorter lengths of launching nose.

(2) With variation in curvature radius R, when the stiffness ratio $k = EJ_1/GJ$ is not very different than 1 (box concrete bridges), the bending moment diagram is not affected by the curvature variation. By contrast, torsion varies significantly, especially for small values of R. Simplified solutions found by straightening the curved box bridge can only be used for bending moment evaluations. For a fixed value of $k > 1$, when R decreases the maximum value of bending moment decreases too, while the torsion increases. For a fixed value of curvature radius R, when k increases, both maximum values of bending moment and torsion decrease.

(3) With variation in stiffness ratio $k = EJ_1/GJ$, keeping R constant, both bending moment and torsion diagrams change, and for smaller values of k (box sections) torsion increases significantly. For higher values of k (open sections with T or I girders) bending moments increase considerably over the pier. In the support section, internal force values can differ a lot, especially at the end of span launching.

(4) With variation in nose length ratio l_n/l, keeping the other parameters constant, the value $l_n/l = 0.60$, indicated as the optimal value for straight bridges, is also confirmed for the torsion effects in curved bridges. Shorter noses show a big increment in bending moment and torsion. For longer noses, forces at the end of launching in the last span are higher than the cantilever ones and the nose length proves not to be advantageous economically.

(5) With variation in the load ratio q_n/q, a significant change can only be appreciated in the first cantilever stage of the span launch, with higher force values for heavier noses. More precise evaluations can be made considering that nose load variations affect its flexural and torsional stiffness, because nose stiffness influences the internal force distribution.

(6) The dimensionless curves of bending moment and torsion maximum values, plotted in the diagrams with variation in both the stiffness ratio k and the curvature radius R, show that the highest values of internal forces are registered in the case of concrete box sections with $R = 100$ m. Moreover, the largest variation in maximum values with the stiffness ratio k is shown by the curve referring to $R = 100$ m. The dimensionless curves provided in this study can be useful for design purposes related to prestressing (axial stresses due to bending moments) and steel reinforcements (tangential stresses due to shear and torsion).

References

[1] Marchetti ME. Specific design problems related to bridges built by using the incremental launching method. Eng Struct 1984;6:185–210.
[2] Rosignoli M. Bridge launching. London: Thomas Telford; 2002.
[3] Calgaro JA, Virlogeux M. Projet et construction des ponts: analyse structurale des tabliers de ponts. Paris: Presses de l'Ecole National de Ponts et Chaussées; 1994.
[4] Manterola Armisen J. Puentes: apuntes para su diseño, cálculo y contrucción. Esc. Tec. Sup. de Ingenieros de Caminos, Canales y Puertos. Madrid; 2006.
[5] Rosignoli M. Misplacement of launching bearings in PC launched bridges. J Bridge Eng ASCE 1998;3(4):170–6.
[6] Rosignoli M. Solution of the continuous beam in launched bridges. Proc Inst Civ Eng Struct Bldgs 1997;122:390–8.
[7] Favre R, Badoux M, Burdet O, Laurencet P. Design of a curved incrementally launched bridge. Struct Eng Int IABSE 1999;2:128–32.
[8] Kristek V. Theory of box girders. NY: John Wiley & Sons; 1979. 372 p.
[9] Arici M, Granata MF. Analysis of curved incrementally launched box concrete bridges using Transfer Matrix Method. Bridge Struct 2007;3(3–4):165–81.
[10] Rosignoli M. Nose–Deck interaction in launched prestressed concrete bridges. J Bridge Eng ASCE 1998;3(1):21–7.
[11] Sasmal S, Ramanjaneyulu K, Srinivas V, Gopalakrishnan S. Simplified computational methodology for analysis and studies on behaviour of incrementally launched continuous bridges. Struct Eng Mech 2004;17(2):245–66.
[12] Fontan AN, Diaz JM, Baldomir A, Hernandez S. Improved optimization formulations for launching nose of incrementally launched prestressed concrete bridges. J Bridge Eng ASCE 2011;16(3):461–70.
[13] Mapelli M, Mola F, Pisani A. Time-dependent analysis of launched bridges. Struct Eng Mech 2006;24(6):741–64.
[14] Jirasek M, Bažant ZP. Inelastic analysis of structures. Chichester: John Wiley & Sons; 2002.
[15] Arici M, Granata MF. A general method for nonlinear analysis of bridge structures. Bridge Struct 2005;1(3):223–44.
[16] Arici M, Granata MF. Generalized curved beam on elastic foundation solved by transfer matrix method. Struct Eng Mech 2011;40(2):279–95.
[17] Sasmal S, Ramanjaneyulu K. Transfer matrix method for construction phase analysis of incrementally launched prestressed concrete bridges. Eng Struct 2006;28:1897–910.
[18] Schlaich J, Scheef H. Concrete box girder bridges. Structural engineering documents IABSE, vol. 1e. Switzerland: IABSE; 1982. 108 p.
[19] AFGC (Association Française de Génie Civil). Guide des ponts poussés. Paris: Presses de l'Ecole National de Ponts et Chaussées; 1999.